Inorganic Chemistry

Article

pubs.acs.org/IC

Unusual Concentration Induced Antithermal Quenching of the Bi^{2+} Emission from $Sr_2P_2O_7$:Bi^{2+}

Liyi Li,[†] Mingying Peng,*[,†] Bruno Viana,[‡] Jing Wang,[§] Bingfu Lei,[∥] Yingliang Liu,[∥] Qinyuan Zhang,[†] and Jianrong Qiu[†]

[†]The China−Germany Research Center for Photonic Materials and Devices, The State Key Laboratory of Luminescent Materials and Devices, and Guangdong Provincial Key Laboratory of Fiber Laser Materials and Applied Techniques, School of Materials Science and Engineering, South China University of Technology, Guangzhou 510641, China

[‡]IRCP Chimie ParisTech, 11 rue Pierre et Marie Curie, 75231 Paris Cedex 05, France

[§]State Key Laboratory of Optoelectronic Materials and Technologies, School of Chemistry and Chemical Engineering, SunYat-Sen University, Guangzhou 510275, China

[∥]The College of Materials and Energy, South China Agricultural University, Guangzhou 510640, China

ABSTRACT: The resistance of a luminescent material to thermal quenching is essential for the application in high power LEDs. Usually, thermal luminescence quenching becomes more and more serious as the activator concentration increases. Conversely, we found here that a red phosphor $Sr_2P_2O_7$:Bi^{2+} is one of the exceptions to this as we studied the luminescence properties at low (10−300 K) and high (300−500 K) temperatures. As Bi^{2+} ions are incorporated into $Sr_2P_2O_7$, they exhibit the emissions at ∼660 and ∼698 nm at room temperature and are encoded, hereafter, as Bi(1) and Bi(2) due to the substitutions for two different crystallographic sites Sr(1) and Sr(2), respectively, in the compound. However, they will not substitute for these sites equally. At lower dopant concentration, they will occupy preferentially Sr(2) sites partially due to size match. As the concentration increases, more Bi^{2+} ions start to occupy the Sr(1) sites. This can be verified by the distinct changes of emission intensity ratio of Bi(2) to Bi(1). As environment temperature increases, the thermal quenching happens, but it can be suppressed by the Bi^{2+} concentration increase. This becomes even more pronounced in Bi^{2+} heavily doped sample as we decompose the broad emission band into separated Bi(1) and Bi(2) Gaussian peaks. For the sample, the Bi(1) emission at ∼660 nm even shows antithermal-quenching particularly at higher temperatures. This phenomenon is accompanied by the blue shift of the overall emission band and almost no changes of lifetimes. A mechanism is proposed due to volume expansion of the unit cell, the increase of Bi(1) content, and temperature dependent energy transfer between Bi(2) and Bi(1). This work helps us better understand the complex luminescent behavior of Bi^{2+} doped materials, and it will be helpful to design in the future the heavily doped phosphor for WLEDs with even better resistance to thermal quenching.

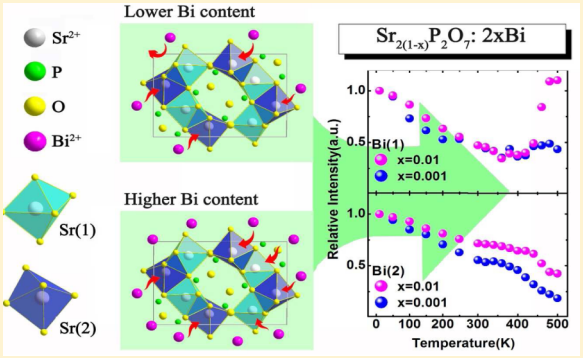

1. INTRODUCTION

Primarily due to the overwhelming advantages as compared to either incandescent or fluorescent lightings such as higher luminous efficiency, longer lifetime, smaller size, and energy saving, white light LEDs (WLEDs)[1−4] have been recognized as the next generation of lighting sources. Lighting world 2013 predicts LEDs will continue dominating the lighting market through 2018, thanks to falling prices, government influences, as well as increasing efficiency. So far, they have found wide applications in domestic and commercial lighting, display technologies, agriculture, medical science, and recently Li-Fi (a new technique of indoor optical wireless communication with incoherent LED lights).[5−12]

At present, phosphor-converted (pc-)WLEDs are one of the most prominent approaches to generate white light. It is usually based on the combination of a single LED chip with one or multiple light-converting phosphors.[1,9,13,14] In the scheme, the chip and the phosphors are two key components, and they determine the eventual performance of the device. In order to produce WLED with warm perception, high color rendering ability, and full color gamut, currently it is still a crucial point to search a red phosphor which can efficiently convert blue or near-ultraviolet (NUV) lights into red, since the (In,Ga)N LED chip in the design can emit lights with wavelengths in either blue (∼450−480 nm) or NUV (∼380−420 nm) ranges.[15−19] Much interest has been focused on rare earth (RE)-based doping schemes, such as Eu^{2+} doped oxynitrides or nitrides.[20−25]

Received: April 21, 2015
Published: May 28, 2015

DOI: 10.1021/acs.inorgchem.5b00887
Inorg. Chem. 2015, 54, 6028−6034

Recently, we have tried a different new approach which is based on nonrare earth and found that bismuth as stabilized in its divalent form in some crystals can emit orange or red lights under the excitation of blue or NUV. Consequently, certain Bi^{2+} doped alkaline earth borates,[26,27] sulfates,[28] phosphates,[29,30] and borophosphates[31] have been reported as promising candidates for red phosphor. Among these, phosphates are considered as one of the suitable hosts for phosphors due to its impressive physical and chemical stability.[32] For a phosphor in WLED, first priority is that it should absorb the lights emitted from the LED chip and then convert them into desirable wavelengths. Particularly for the phosphor which applies to NUV chips, it will be ideal that it can fully absorb all the lights from the chips, and it can guarantee no leakage of ultraviolet lights. Otherwise, when the lamp was used, long time exposure of a human to the leaked ultraviolet lights would cause serious consequences, such as raising the risk of skin cancer.[33] To increase the sample absorbance, one of the natural solutions is to increase the concentration of activator in the sample according to Lambert's law.[34] This usually leads to the concentration or even severe thermal quenching. The trade-off has to be balanced between the concentration and the quenching.

It has been noticed that, as high power WLED works, the temperature of the layer deposited on the chip can rise to more than 150 °C, which comes from the heat rouse from the p−n junction and the phosphor layer.[35] This inspires us to investigate the resistance of the luminescence from the phosphor candidate to the thermal impact, since the thermal stability is a vital factor to the WLEDs for their application. So far there have been no reports on high temperature luminescent properties of Bi^{2+} doped phosphors, e.g., $Sr_2P_2O_7:Bi^{2+}$. Normally at higher temperature, as the concentration of activator increases, thermal quenching becomes more prominent, which is reflected by the drastic reduction of both photoluminescence (PL) intensity and lifetime. One of the vivid instances is YAG:Ce by Meijerink et al.[36] There have been few reports on suppression of thermal quenching by the increase of dopant concentration.

In this paper, we will report an exception on this in the phosphor $Sr_2P_2O_7:Bi^{2+}$. We will employ different types of instrumentations such as X-ray diffraction, Rietveld refining, static and dynamic excitation, emission spectra and lifetimes at lower temperature (10 to 300 K) and higher temperature (300 to 500 K), etc. to illustrate the phenomenon and unravel the nature of it. The mechanism will be discussed at the end on how the antithermal quenching occurs especially for the emission center of Bi(1) in the heavily doped samples.

2. EXPERIMENTAL SECTION

2.1. Sample Synthesis. Doped and undoped samples of $Sr_{2(1-x)}P_2O_7:2xBi$ (x = 0, 0.001, 0.003, 0.005, 0.01, 0.02, 0.03, and 0.05) were synthesized by conventional solid state reactions at high temperatures. The starting materials were analytical grade reagents $SrCO_3$, $NH_4H_2PO_4$, and Bi_2O_3. The mixtures were preheated at 500 °C for 6 h in air to slowly decompose the ammonium dihydrogen phosphates. This can prevent foaming in consequent calcinations. After thorough grinding, the samples were sintered at 1100 °C for 24 h in air. In order to promote the reduction of bismuth from trivalent to divalent bismuth, the samples were annealed at 1100 °C for 1 h in a reducing CO atmosphere.[31]

2.2. Characterization. The phase purity of all samples was checked by X-ray diffraction (XRD, Rigaku D/max-IIIA, Cu Kα radiation, 40 kV, 40 mA, 1.2° min^{-1}, λ = 1.5405 Å) at room temperature. Excitation and emission spectra as well as decay curves were measured by a high-resolution spectrofluorometer (Edinburgh FLS 920) equipped with a red-sensitive photomultiplier (Hamamatsu R928P) at 10−300 K (in a closed cycle helium cryostat) and 300−500 K (in a high-temperature cell). Excitation curves were corrected over the lamp intensity with a silicon photodiode, and the emission curves were corrected from the PMT spectral response.

3. RESULTS AND DISCUSSION

3.1. Phase Identification of $Sr_2P_2O_7:Bi^{2+}$. XRD results show all samples are single phase of $Sr_2P_2O_7$. Figure 1 shows

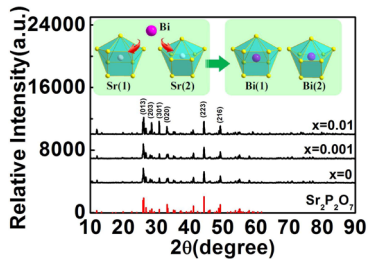

Figure 1. XRD pattern of $Sr_{2(1-x)}P_2O_7:2xBi$ (x = 0, 0.001, and 0.01) and the diffraction peaks of $Sr_2P_2O_7$ from Jade 5.0 PDF #13-0194 included at the bottom of the figure for reference.

for instance the XRD patterns for undoped and bismuth doped samples of $Sr_{2(1-x)}P_2O_7:2xBi$ (x = 0, 0.001, and 0.01). They are consistent with the diffraction peaks of $Sr_2P_2O_7$ derived from Jade 5.0, which are enclosed for reference in the figure. Rietveld refining reveals all samples crystallized in the orthorhombic system with space group *Pnma*. The refining also produces the lattice parameters a = 8.9168(3) Å, b = 5.4005(4) Å, c = 13.1665(4) Å for the sample x = 0, and a = 8.9298(7) Å, b = 5.4016(9) Å, c = 13.1808(1) Å for the sample x = 0.005, and a = 8.9405(3) Å, b = 5.4126(1) Å, c = 13.1864(2) Å for the sample x = 0.01. The parameters increase as bismuth content x increases. This agrees with the shift of the diffraction peaks toward lower angle and it should be due to the successful substitution of bismuth for strontium as the inset of Figure 1 shows. It at the same time means the radius of Bi^{2+}, which has never been reported so far, should be a little larger than Sr^{2+} in same coordination field. We can get the hint from the comparison between Bi^{+} and Sr^{2+} radii which are 1.808 and 1.31 Å, respectively, with coordination number of 9.[37,38]

Refining shows there are two distinct Sr^{2+} lattice sites in the compound, both of which are coordinated by nine oxygen atoms. The average bond length for Sr−O is 2.7214 and 2.6794 Å for Sr(1) and Sr(2), respectively. Calculation based on the dielectric chemical bond theory indicates the mean chemical bond covalency f_c is 0.1209 for Sr(1)−O and 0.1215 for Sr(2)−O, respectively.

3.2. Photoluminescence of $Sr_2P_2O_7:Bi^{2+}$ at Room Temperature. Figure 2 depicts the emission spectra of $Sr_2P_2O_7:Bi^{2+}$ samples for different Bi concentrations at room temperature. Upon the excitation at 272 nm, a broad emission was observed spanning from 600 to 800 nm and peaking at ∼698 nm with a fwhm (full width at half-maximum) of more than 1069 cm^{-1}, which is due to the transition of $^2P_{3/2}(1) \rightarrow {}^2P_{1/2}$ of the divalent bismuth ions. The emission intensity is intensified by about two times as the content of bismuth x increases from 0.001 to 0.01. It is quenched by about three times as x continues increasing from 0.01 to 0.05. This means the optimal Bi^{2+} concentration as 0.01 in $Sr_2P_2O_7$: Bi^{2+}.

DOI: 10.1021/acs.inorgchem.5b00887
Inorg. Chem. 2015, 54, 6028−6034

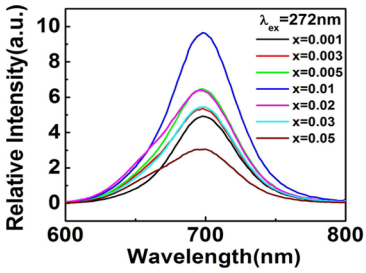

Figure 2. Emission spectra of $Sr_{2(1-x)}P_2O_7$:2xBi (x = 0.001, 0.003, 0.005, 0.01, 0.03, and 0.05) under the excitation of 272 nm.

To well understand the quenching mechanism, we calculated the critical distance R_c for the energy transfer in $Sr_2P_2O_7$:Bi^{2+} at the critical concentration x_c with[39]

$$R_c = \sqrt[3]{6V/(\pi x_c N)} \quad (1)$$

where N is the number of strontium sites in unit cell and V represents the cell volume. The value of N and V can be obtained from phase data of crystallographic structure analysis. Here x_c = 1.0%, N = 4, V = 544 Å, R_c is, thus, estimated to be as high as 29.6 Å. Generally, the nonradiative energy transfer may result from multipolar interaction and possibly exchange mechanisms at short distances. However, in this work, the value of R_c is much larger than the typical critical distance for the exchange interaction (about 5 Å).[40] This means that the concentration quenching behavior can be attributed to the nonradiative electric multipolar interaction or defect centers which could appear at higher concentrations.

The possibility of multipolar energy transfer mechanism can be written as the following equation given by Van Uitert:[41]

$$I = X[k/(1 + \beta(x/x_c')^{\theta/3})] \quad (2)$$

where k and β are constants; the emission intensity I is dependent on concentration x; x'_c = 1.0% is the critical concentration; and the value of θ could be 6, 8, or 10, which represents electric dipole−dipole, dipole−quadrupole, and quadrupole−quadrupole interaction, respectively. Fitting the integrated emission intensity vs the concentration x with eq 2 by taking θ = 6, 8, or 10 produces the correlation coefficiency of 98.9%, 94.7%, or 80.6%, respectively. The fittings are illustrated as Figure 3 along with the experimental results. So, these imply that the electric dipole−dipole interaction might dominate the quenching process of Bi^{2+} photoluminescence in $Sr_2P_2O_7$:Bi^{2+}.

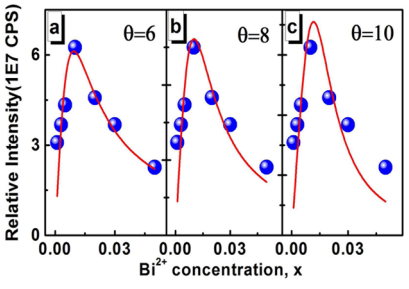

Figure 3. Dependence of Bi^{2+} concentration on emission intensity in $Sr_2P_2O_7$:Bi. Fitting the dependence by eq 2 with θ = 6, 8, and 10, produces the red curves in (a), (b), and (c), respectively. The fitting parameters are (a) k = 210 ± 35.12, β = 1.15 ± 0.32, θ = 6, R_{sq} = 98.9%; (b) k = 179 ± 30.3, β = 1.67 ± 0.53, θ = 8, R_{sq} = 94.7%; (c) k = 146 ± 28.1, β = 2.55 ± 0.11, θ = 10, R_{sq} = 80.6%.

By inspecting Figure 2 carefully, we can find that, though the peak position does not shift as x increases, the shape of the peak changes from symmetry to asymmetry especially at higher energy side. The peak can be well discomposed into two Gaussian peaks at ∼660 and ∼698 nm. Monitoring the emissions at these peaks leads to different excitation spectra as in Figure 4. For the emission at ∼698 nm, the excitation peaks

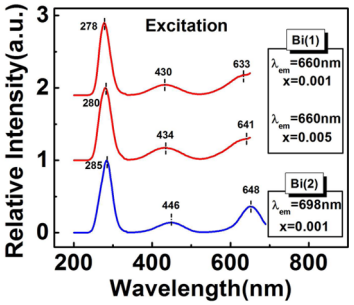

Figure 4. Excitation spectra of $Sr_{2(1-x)}P_2O_7$:2xBi (x = 0.001 and 0.005) monitored at the emissions at 660 (red lines) and 698 nm (blue line) at room temperature.

were observed at 285, 446, and 648 nm, respectively. The peaks keep unshifted as x changes. For the emission at ∼660 nm, the excitation peaks lie at 278, 430, and 633 nm when the content x is lower, and they move to 280, 434, and 641 nm as x increases to 0.05. The results show that these emissions should be from different centers. On basis of crystallographic data, the emission at ∼660 nm can be assigned to Bi(1) which substitutes for Sr(1) while the emission at ∼698 nm is from Bi(2) residing at Sr(2). The excitation peaks in the blue and red ranges are due to the Bi^{2+} transitions from $^2P_{1/2}$ to $^2P_{3/2}(2)$ and $^2P_{3/2}(1)$, respectively. The UV excitation peak used to be assigned to the transition from $^2P_{1/2}$ to $^2S_{1/2}$. However, recent calculation shows it should come from the ground state to $6s6p^2$ (^4P) and doublets of the configurations $6s6p^2$, $6s^26d$, and $6s^26p$.[42]

3.3. Site Occupancy Preference of Bi^{2+} Ions in $Sr_2P_2O_7$:Bi^{2+}. When the temperature is lowered to 10 K, the broad emission band of Bi^{2+} as shown in Figure 2 degrades into two well-resolved peaks at ∼660 and ∼698 nm from the centers of Bi(1) and Bi(2), respectively. The change has been illustrated in Figure 5, and it has been found in the samples doped with different content of bismuth. As excitation goes into 450 nm (corresponding to Bi(2) absorption), besides the expected Bi(2) emission at ∼698 nm, the Bi(1) emission was

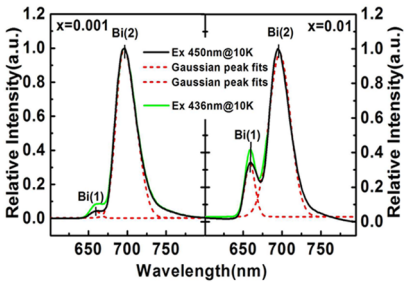

Figure 5. Emission spectra of $Sr_{2(1-x)}P_2O_7$:2xBi (x = 0.001 and 0.01) measured at 10 K upon the excitations at 450 and 436 nm, respectively. Dotted curves are the Gaussian peak decomposition results for the emission spectra corresponding to the excitation at 450 nm.

DOI: 10.1021/acs.inorgchem.5b00887
Inorg. Chem. 2015, 54, 6028−6034

observed at ~660 nm. This implies the possible energy transfer from Bi(2) to Bi(1), and it can be evidenced further by the excitation spectra at 10 K, which is depicted in Figure 6. The

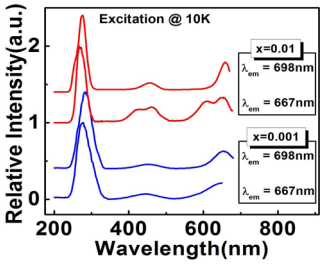

Figure 6. Excitation spectra of $Sr_{2(1-x)}P_2O_7$:2xBi (x = 0.001 and 0.01) by monitoring the emissions at 667 and 698 nm at 10 K, respectively.

excitation spectrum of the emission from Bi(1) at ~660 nm consists of the excitation peaks at 270, 422, 463, 608, and 652 nm in the sample x = 0.01. Comparison to the excitation spectrum of the emission at ~698 nm from Bi(2) shows that the peaks at 463 and 652 nm are from Bi(2). Therefore, the energy transfer happens from Bi(2) to Bi(1).

When the excitation was made by a shorter wavelength such as 436 nm, the intensity of Bi(1) emission at ~660 nm is intensified a little, but it is still much weaker than the emission at ~698 nm from Bi(2). We notice that, for the sample x = 0.001, the intensity ratio of Bi(2) emission to Bi(1) emission is about 34.16 upon the excitation plan of 450 nm, and the ratio changes to 3.26 for the sample x = 0.01. This reveals two things. One is that once Bi^{2+} ions are doped into the compound they will not enter the two sites of Sr(1) and Sr(2) with the same statistic possibility though they are similarly coordinated by nine oxygen atoms. Since the critical concentration of Bi^{2+} is ~0.01 as mentioned above, the emission intensity is approximately proportional to the content x of Bi^{2+} as x is less than 0.01. The much stronger Bi(2) emission in the sample x = 0.001 means that Bi^{2+} ions will preferentially substitute for Sr(2) rather than Sr(1). This perhaps is driven by the more desirable size match between Bi^{2+} and Sr(2). The similarity in the excitation spectra of the Bi(1) and Bi(2) emissions of the sample x = 0.001 supports also the conclusion (see Figure 6) that most of Bi^{2+} ions reside at the sites of Bi(2).

Another conclusion is that Bi^{2+} ions start to substitute for Sr(1) sites as x increases. As a consequence, the emission intensity from Bi(1) sites increases, and it leads to the significant decrease of the intensity ratio of Bi(2) emission to Bi(1) emission. Meanwhile, the excitation spectrum of the Bi(1) 660 nm emission changes and the typical excitation peaks show up due to the Bi(1) centers (see Figure 6).

3.4. Concentration Induced Antithermal Quenching of the Bi^{2+} Emissions from $Sr_2P_2O_7$:Bi^{2+} at a Lower Temperature Range (10–300 K). Figure 7 shows the emission spectra of $Sr_{2(1-x)}P_2O_7$:2xBi (x = 0.001 and 0.01) at different temperatures which change between 10 and 300 K. Generally speaking, as you can see from Figure 7, the intensity of the emissions decreases upon the excitation at 450 nm as the temperature increases. At the same time the Bi(1) emission at ~660 nm gradually immerges into the Bi(2) emission at ~698 nm, and the emission is thermally broadened (for instance for the sample x=0.01, fwhm of the ~698 nm emission changes from 31 to 60 nm when the temperature increases to 300 from 10 K) and it red shifts slightly. The slight redshift of the ~698

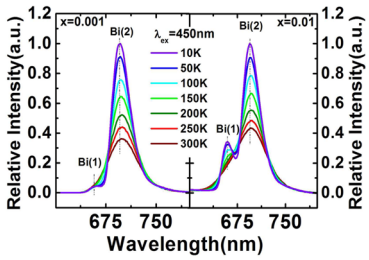

Figure 7. Emission spectra of $Sr_{2(1-x)}P_2O_7$:2xBi (x = 0.001 and 0.01) measured at 10–300 K upon the excitation at 450 nm.

nm emission peak along with temperature is possibly due to the enhanced interaction between Bi^{2+} ions and host. This is reflected further by the increase of splitting energy between $^2P_{3/2}(1)$ and $^2P_{3/2}(2)$. The splitting is 6707 cm^{-1} at 10 K, and it increases to 6937 cm^{-1} at 300 K (see Figure 8).

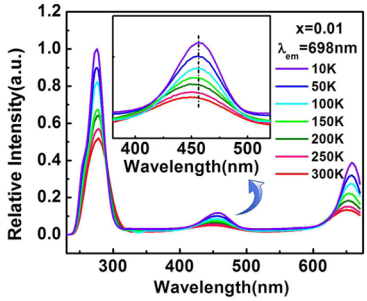

Figure 8. Excitation spectra of $Sr_{2(1-x)}P_2O_7$:2xBi (x = 0.01) at different temperatures by monitoring the emission at 698 nm in the temperature range from 10 to 300 K.

As we decomposed the emission spectra into two Gaussian peaks at ~660 and 698 nm, which correspond to Bi(1) and Bi(2), respectively, and plotted the integrated intensity of each peak against temperature, we noticed that, though the general trend is decreasing for all the samples in the range of 10–300 K, the decrease rate is very different for the samples doped with different Bi content. The decrease rate will be slowed as the content x increases. Figure 9 exemplarily shows the direct comparison between the samples x = 0.001 and 0.01. This concentration-induced antithermal quenching has seldom been noticed before.

3.5. Concentration Induced Antithermal Quenching of the Bi^{2+} Emissions from $Sr_2P_2O_7$:Bi^{2+} at a Higher

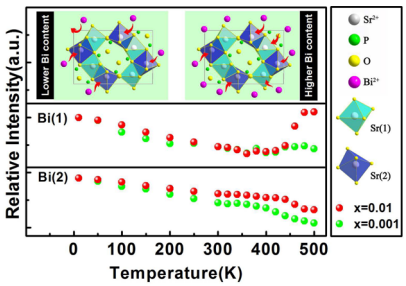

Figure 9. Temperature dependence of integrated emission intensity of Bi(1) and Bi(2) in $Sr_{2(1-x)}P_2O_7$:2xBi (x = 0.001, red dotted curves; x = 0.01, green dotted curves) between 10 and 500 K. Insets illustrate the site occupancy preference of Bi^{2+} in the cases of lower and higher bismuth contents, respectively.

DOI: 10.1021/acs.inorgchem.5b00887
Inorg. Chem. 2015, 54, 6028–6034

Temperature Range (300−500 K). Normally, thermal quenching becomes worse as the dopant content increases. Our observation is obviously contradictory to this. The sample with higher concentration exhibits a better thermal resistance compared to the lower concentration sample. This becomes more predominant at higher temperatures, and it can be supported by Figure 10, which illustrates the emission spectra

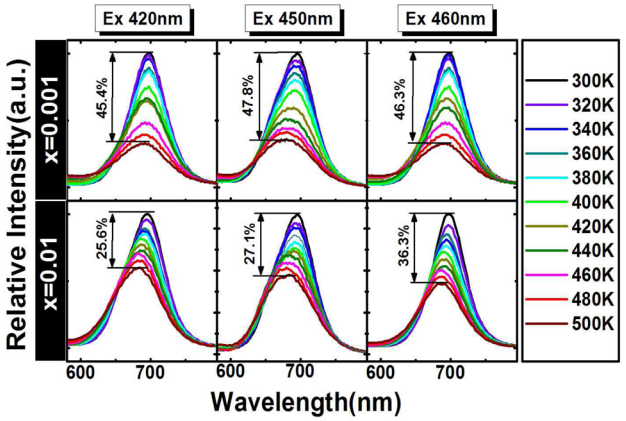

Figure 10. Emission spectra of $Sr_{2(1-x)}P_2O_7$:2xBi (x = 0.001 and 0.01) upon the excitations at 420, 450, and 460 nm at the temperature ranging from 300 to 500 K.

for $Sr_{(1-x)}P_2O_7$:2xBi (x = 0.001 and 0.01) under the excitations at 420, 450, and 460 nm recorded at the temperatures higher than 300 K, respectively. As temperature increases from 300 to 500 K, the emission intensity of sample x = 0.001 decreases by 47.8%, and the intensity decreases by 27.1% for sample x = 0.01 upon the excitation of 450 nm. The quenching becomes also lowered upon different blue excitations in the samples x = 0.005, 0.01, and 0.05, respectively, when compared to the sample x = 0.001 (see Figure 11). As further dividing the broad

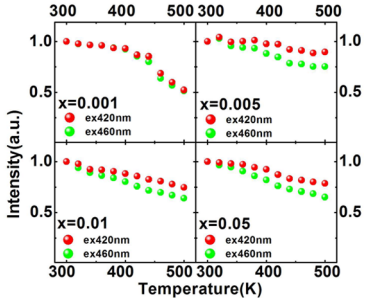

Figure 11. Temperature dependence of integrated emission intensity of $Sr_{2(1-x)}P_2O_7$:2xBi (x = 0.001, 0.005, 0.01, and 0.05) upon the excitations at 420 and 460 nm at a temperature from 300 to 500 K.

emission into the Bi(1) and Bi(2) emissions at ∼660 and 698 nm, respectively, by Gaussian peak splitting fitting, we plotted the intensity dependence of the Bi(1) and Bi(2) emissions on temperature and concentration in Figure 9. The rate of intensity decrease along temperature becomes much slower at higher content of Bi for different blue excitations (see Figure 10). This is applicable to the emission centers of Bi(1) and Bi(2). As the temperature rises from 400 to 500 K, the emission intensity of Bi(1) increases rather than decreases at the earlier state for the sample x = 0 .001, and it is even enhanced by more than two times in sample x = 0.01 (see Figure 9). So the emission center of Bi(1) exhibits better resistance to thermal impact than Bi(2).

Figure 12a,b depicts the luminescence decay curves of Bi(1) and Bi(2) for $Sr_{2(1-x)}P_2O_7$:2xBi (x = 0.001, 0.005, 0.01, and

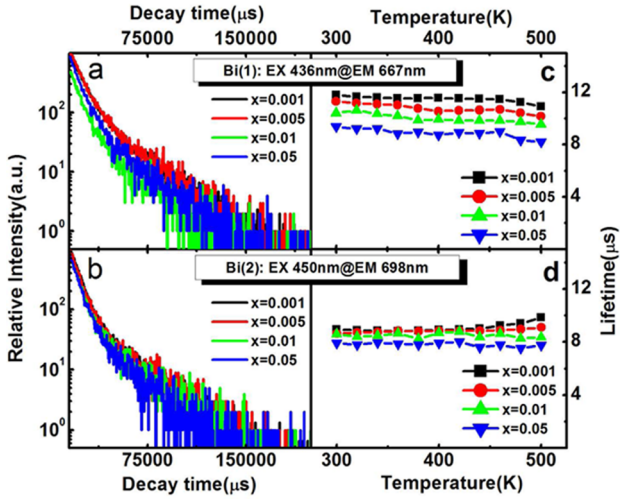

Figure 12. Luminescence decay curves for $Sr_{2(1-x)}P_2O_7$:2xBi (x = 0.001, 0.005, 0.01, and 0.05): (a) λ_{ex} = 436, λ_{em} = 667 nm and (b) λ_{ex} = 450, λ_{em} = 698 nm at 300 K. Temperature dependence of lifetime for $Sr_{2(1-x)}P_2O_7$:2xBi (x = 0.001, 0.005, 0.01, and 0.05): (c) λ_{ex} = 436, λ_{em} = 667 nm and (d) λ_{ex} = 450, λ_{em} = 698 nm.

0.05) at different temperatures, and Figure 12c,d shows the dependence of the lifetime of the Bi(1) and Bi(2) emissions on temperature. As we can observe in Figure 12, for both Bi(1) and Bi(2) sites, the decay time is temperature independent. However, it varies as a function of Bi concentration. For the Bi(1) site, the decay time varies in the range 9.0−11.5 μs, while for the Bi(2) site, the decay time varies in the range 8.0−9.0 μs.

3.6. Mechanism for Concentration Induced Antithermal Quenching of the Bi^{2+} Emissions from $Sr_2P_2O_7$:Bi^{2+}.

Contrary to the case at lower temperature (10−300 K), Bi^{2+} emission shifts toward shorter wavelengths at higher temperature (300−500 K, Figure 10). Though thermal quenching occurs, it can be slowed once higher content of bismuth is introduced into the samples. The effect of concentration on antithermal quenching of the Bi^{2+} emission can be enhanced at higher temperatures. In the following, we will try to elucidate how all these phenomena happen.

Once bismuth is doped into the compound, it will unavoidably experience the crystal field local oxygen atoms around bismuth create. Since we have known that the naked valence electrons of bismuth are very susceptible to the changes of local field around bismuth,[26−31] the tiny changes of the field will be directly reflected by the response of Bi^{2+} luminescence to temperature or concentration. As temperature increases, the coupling interaction between Bi^{2+} and matrix might be strengthened by the enhanced vibration of the Bi−O bond, and it also might be weakened by the elongation of Bi−O bond length due to the expansion of the lattice cell. Whether the overall interaction increases or not depends on the trade-off between the Bi−O bond vibration and elongation. At lower temperature which ranges from 10 to 300 K, the bond vibration enhancement might dominate over the elongation. So, the interaction will be enhanced as the temperature increases, and it will lower the energy level of the first excited state of $^2P_{3/2}(1)$.

DOI: 10.1021/acs.inorgchem.5b00887
Inorg. Chem. 2015, 54, 6028−6034

Therefore, as Figures 7 and 8 depict, the emission red shift was observed along with the increase of the splitting energy between $^2P_{3/2}(1)$ and $^2P_{3/2}(2)$.

At higher temperature range from 300 to 500 K, the bond length elongation due to cell expansion might dominate over the bond vibration. So, the crystal field will be weakened with the increase of the temperature around bismuth. This might partially contribute to the blue shift of the overall emission peak (see Figure 10). Another aspect which leads to the emission blueshift might be due to the energy transfer from Bi(2) to Bi(1). The process can be promoted by the increase in either temperature or concentration. It is also responsible for the abnormal enhancement of Bi(1) at higher temperature and higher concentration (see Figure 9). The energy transfer might be the reason why the lifetime of Bi(1) emission is slightly longer than Bi(2) for the same concentration of Bi doped sample (see Figure 12).

Compared with other concentration samples, the temperature quenching of the lowest concentration (x = 0.001) is more pronounced. Other samples perform a better resistance against thermal quenching. This may be attributed to the increased contribution of Bi(1) type luminescent centers. As discussed above, the energy will transfer, rather than quenching, from Bi(2) to Bi(1) with temperature increased. For a lower concentration, the Bi ion will be hardly incorporated into Sr(1). So the energy will transfer less efficiently than that of a higher concentration. That is, Bi(1) type luminescent centers will limit the temperature quenching. Among all the compounds, the sample under excitation at 436 nm with x = 0.005 presents the best resistance against temperature quenching. The emission intensity remains 78.7% of the maximum intensity when the temperature rises from 300 to 500 K. The quenching temperature $T_{50\%}$ cannot be determined here due to the experimental limitation. However, it should be far beyond 500 K as Figure 10 illustrates.

Figure 13 shows the temperature dependence of integrated emission intensity for sample x = 0.005 under the excitation at 436 nm. According to the classical theory of thermal quenching, the temperature-dependent PL intensity can be described by the following equation:[43]

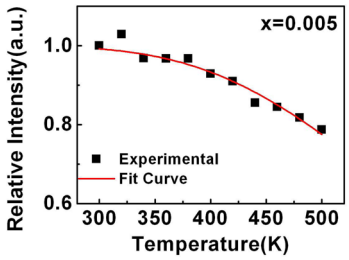

Figure 13. Temperature dependence of integrated emission intensity of $Sr_{2(1-x)}P_2O_7$:2xBi (x = 0.005) upon the excitation at 436 nm. The red line is the fitting results by eq 3 with A = 174 ± 15, ΔE = 0.310 ± 0.039 eV, R_s = 94.5%.

$$I(T) = I_0/(1 + A\ \exp(-\Delta E/kT)) \quad (3)$$

where $I(T)$ is the intensity at temperature T, I_0 is the initial intensity, A is the frequency factor which is the adjustable parameter, k is the Boltzmann constant, and ΔE is the activation energy for the thermal quenching process. As seen in Figure 13, the experimental data are well fitted by eq 3. The ΔE values are obtained to be 0.31 eV for excitation at 436 nm. The quenching can be understood in the framework of the configurational coordination scheme. The luminescence might be quenched by thermally activated crossover from the first excited state of $^2P_{3/2}(1)$ to the ground state $^2P_{1/2}$. This can explain why the emission intensity is weakened. The slowing of thermal quenching in the sample doped with a higher concentration of bismuth might also be partially due to the expansion of the unit cell along bismuth addition.

4. CONCLUSIONS

Unusual concentration induced antithermal quenching of divalent bismuth ions was observed in Bi^{2+} heavily doped $Sr_2P_2O_7$ phosphors along with the blueshift of the emission peak at higher temperature. This is considered due to the unit cell expansion, the increase of Bi (1) content, and the enhanced energy transfer from Bi(2) to Bi(1). The phenomena have been seldom reported, and they are very different from what general thoughts should be on thermal quenching. As the bismuth content is low, Bi^{2+} ions will prefer incorporating into Sr(2) rather than Sr(1) due to radius match, and they start to occupy Sr(1) sites at higher content of bismuth. This leads to the quite high quenching temperature (>500 K) in the heavily doped sample. We believe this work is helpful to design the heavily doped phosphor for WLEDs with better resistance to thermal quenching and excitation light leakage, which will reduce the risk to expose under unhealthy lights in the future.

AUTHOR INFORMATION

Corresponding Author

*E-mail: pengmingying@scut.edu.cn.

Notes

The authors declare no competing financial interest.

ACKNOWLEDGMENTS

This work was financially supported by National Natural Science Foundation of China (Grant Nos. 51322208 and 51132004), Guangdong Natural Science Foundation for Distinguished Young Scholars (Grant No. S20120011380), the Department of Education of Guangdong Province (Grant No. 2013gjhz0001), and Fundamental Research Funds for the Central Universities.

REFERENCES

(1) Schubert, E. F.; Kim, J. K. *Science* **2005**, *308*, 1274−1278.
(2) Zhang, R.; Lin, H.; Yu, Y. L.; Chen, D. Q.; Xu, J.; Wang, Y. S. *Laser Photonics Rev.* **2014**, *8*, 158−164.
(3) Xie, R. J.; Hirosaki, N.; Suehiro, T.; Xu, F. F.; Mitomo, M. *Chem. Mater.* **2006**, *18*, 5578−5583.
(4) Pimputkar, S.; Speck, J.; DenBaars, S.; Nakamura, S. *Nat. Photonics* **2009**, *3*, 180−181.
(5) Chen, D. Q.; Wang, Y. S.; Zheng, K. L.; Guo, T. L.; Yu, Y. L.; Huang, P. *Appl. Phys. Lett.* **2007**, *91*, 251903−1−3.
(6) Xia, Z.; Zhuang, J.; Meijerink, A.; Jing, X. *Dalton Trans.* **2013**, *42*, 6327−6336.
(7) Dai, P. P.; Zhang, X. T.; Bian, L. L.; Lu, S.; Liu, Y. C.; Wang, X. J. *J. Mater. Chem. C* **2013**, *1*, 4570−4576.
(8) Lu, W.; Zhang, X.; Wang, Y.; Hao, Z. D.; Liu, Y. F.; Luo, Y. S.; Wang, X. J.; Zhang, J. H. *J. Alloys Comp.* **2012**, *513*, 430−435.
(9) Peng, M. Y.; Yin, X. W.; Tanner, A. T.; Brik, M. G.; Li, P. F. *Chem. Mater.* **2015**, *27*, 2938−2945.
(10) Yang, X. F.; Song, H. L.; Yang, L. X.; Xu, X. *J. Am. Ceram. Soc.* **2011**, *94*, 164−171.
(11) Sewaiwar, A.; Tiwari, S.; Chung, Y. *Opt. Commun.* **2015**, *339*, 153−156.

DOI: 10.1021/acs.inorgchem.5b00887
Inorg. Chem. 2015, 54, 6028−6034

(12) Law, G. L.; Wong, K. L.; Tam, H. L.; Cheah, K. W.; Wong, W. T. *Inorg. Chem.* **2009**, *48*, 10492−10494.
(13) Qin, C. X.; Huang, Y. L.; Shi, L.; Chen, G. Q.; Xiao, X. B.; Seo, H. J. *J. Phys. D: Appl. Phys.* **2009**, *42*, 185105.
(14) Jia, Y. C.; Lv, W.; Guo, N.; Lv, W. Z.; Zhao, Q.; You, H. P. *Chem. Commun.* **2013**, *49*, 2664−2666.
(15) Park, J. K.; Choi, K. J.; Kim, C. H.; Park, H. D.; Park, J. T.; Choi, S. Y. *Electrochem. Solid-State Lett.* **2004**, *7*, H15.
(16) Inoue, K.; Hirosaki, N.; Xie, R. J.; Takeda, T. *J. Phys. Chem. C* **2009**, *113*, 9392−9397.
(17) Zhang, G.; Wang, J.; Chen, Y.; Su, Q. *Opt. Lett.* **2010**, *35*, 2382−2384.
(18) Guo, C. F.; Xu, Y.; Lv, F.; Ding, X. *J. Alloys Comp.* **2010**, *297*, L21−L24.
(19) Kim, J. S.; Kang, J. Y.; Jeon, P. E.; Chol, J. C.; Park, H. L.; Kim, T. W. *Jpn. J. Appl. Phys.* **2004**, *43*, 989−992.
(20) Li, Y. Q.; Delsing, A. C. A.; de With, G.; Hintzen, H. T. *Chem. Matter.* **2005**, *17*, 3242−3248.
(21) Liu, X. M.; Lin, C. K.; Lin, J. *Appl. Phys. Lett.* **2007**, *90*, 081904.
(22) Saradhi, M. P.; Varadaraju, U. V. *Chem. Mater.* **2006**, *19*, 5267−5272.
(23) Setlur, A. A.; Heward, W. J.; Hannah, M. E.; Happek, U. *Chem. Matter.* **2008**, *20*, 6277−6283.
(24) Bandi, W. R.; Grandhe, B. K.; Woo, H. J.; Jang, K.; Shin, D. S.; Yi, S. S.; Jeong, J. H. *J. Alloys. Comp.* **2012**, *538*, 85−90.
(25) Smedskjaer, M.; Wang, J.; Yue, Y. *J. Mater. Chem.* **2011**, *21*, 6614−6620.
(26) Peng, M. Y.; Wondraczek, L. *J. Am. Ceram. Soc.* **2010**, *93*, 1437−1442.
(27) Peng, M. Y.; Wondraczek, L. *Opt. Lett.* **2009**, *34*, 2885−2887.
(28) Cao, R. P.; Peng, M. Y.; Qiu, J. R. *Opt. Express* **2012**, *20*, A977−A983.
(29) Peng, M. Y.; Sprenger, B.; Schmidt, M. A.; Schwefel, H. G. L.; Wondraczek, L. *Opt. Express* **2010**, *18*, 12852−12863.
(30) Peng, M. Y.; Wondraczek, L. *Opt. Lett.* **2010**, *35*, 2544−2546.
(31) Peng, M. Y.; Da, N.; Krolikowski, S.; Stiegelschmitt, A.; Wondraczek, L. *Opt. Express* **2009**, *17*, 21169−21178.
(32) Peng, M. Y.; Lei, J. C.; Li, L. Y.; Wondraczek, L.; Zhang, Q. Y.; Qiu, J. R. *J. Mater. Chem. C* **2013**, *1*, 5303−5308.
(33) Clydesdale, G.; Dandie, G.; Muller, H. *Immunol. Cell Biol.* **2001**, *79*, 547−568.
(34) Gore, M. G. *Spectrophotometry and Spectrofluorimetry: A Practical Approach*; Oxford University Press: New York, 2000.
(35) Kang, F. W.; Peng, M. Y.; Zhang, Q. Y.; Qiu, J. R. *Chem.—Eur. J.* **2014**, *20*, 11522−11530.
(36) Bachmann, V.; Ronda, C.; Meijerink, A. *Chem. Mater.* **2009**, *21*, 2077−2084.
(37) Shannon, R. D. *Acta Crystallogr.* **1967**, *A32*, 751−767.
(38) Romanov, A.; Grigoriev, F.; Sulimov, V. *Comput. Theor. Chem.* **2013**, *1017*, 159−161.
(39) Blasse, G.; Grabmaier, B. *Luminescent Materials*; Springer Verlag: Berlin, 1994.
(40) Kang, F. W.; Peng, M. Y.; Yang, X. B.; Dong, G. P.; Nie, G. C.; Liang, W. J.; Xu, S. H.; Qiu, J. R. *J. Mater. Chem. C* **2014**, *2*, 6068−6076.
(41) Van Uitert, L. *J. Electrochem. Soc.* **1967**, *114*, 1048−1053.
(42) Mathijs, D. J.; Meijerink, A.; Gordon, R. A.; Barandiaran, Z.; Seijo, L. *J. Phys. Chem. C* **2014**, *118*, 9696−9705.
(43) Wang, J.; Zhang, M.; Zhang, Q.; Ding, W.; Su, Q. *Appl. Phys. B: Laser Opt.* **2007**, *87*, 249−254.

DOI: 10.1021/acs.inorgchem.5b00887
Inorg. Chem. 2015, 54, 6028−6034